THE JOURNAL OF PHYSICAL CHEMISTRY B

 VOLUME 108, NUMBER 50, DECEMBER 16, 2004

LETTERS

Precise Electronic $\chi^{(2)}$ Spectra of Molecules Adsorbed at an Interface Measured by Multiplex Sum Frequency Generation

Shoichi Yamaguchi and Tahei Tahara*

Molecular Spectroscopy Laboratory, RIKEN (The Institute of Physical and Chemical Research), 2-1 Hirosawa, Wako, Saitama 351-0198, Japan

Received: October 14, 2004; In Final Form: November 7, 2004

We have developed a new technique to obtain a second-order nonlinear ($\chi^{(2)}$) electronic spectrum of molecules adsorbed at an interface. This technique is based on multiplex sum frequency generation that utilizes femtosecond near-infrared pulses and white light continuum. We obtained the $|\chi^{(2)}|^2$ spectra of a dye Nile Blue (NB) at the air/water interface with an unprecedented high signal-to-noise ratio and dense wavelength data points. Fitting analyses with an exact $\chi^{(2)}$ expression were performed for the spectra, and detailed information about the electronic structure of NB at the interface was obtained.

Introduction. Second-order nonlinear spectroscopy is known as a powerful tool to study the structure and dynamics of molecules at interfaces that are very important in fundamental science and industrial application.[1] Vibrational spectra of interfacial molecules are measured by IR−visible (vis) sum frequency generation (SFG) spectroscopy that has been widely utilized since the first demonstration of $\chi^{(2)}$ (second-order nonlinear susceptibility) IR spectra by Shen and co-workers.[2] The sensitivity of the IR−vis SFG spectroscopy has been improved to a great extent by using broadband IR pulses and multichannel detectors,[3−6] and high-quality IR−vis SFG spectra can be measured nowadays. Recently, fourth-order Raman spectroscopy in the time domain was introduced as another method to obtain interface-specific vibrational spectra.[7−9] On the other hand, electronic $\chi^{(2)}$ data of interfacial molecules are measured by the resonance second harmonic generation (SHG) method. In the spectral measurements, the SHG light intensity is recorded point by point with scanning the fundamental excitation wavelength, and this technique has not been changed since Heinz et al. first reported the SHG spectra of dye molecules on silica.[10] Because interface-specific electronic spectra are indispensable for the studies of molecular orientation,[11,12] rotation,[13,14] solvation,[15,16] polarity,[17,18] and the other static and dynamic properties at interfaces,[1,19−26] it is highly desirable to obtain precise electronic $\chi^{(2)}$ spectra. However, it is difficult to measure high-quality electronic spectra of interfacial molecules by the conventional scanning method.

We have noted that the recent advances of femtosecond lasers can bring the multiplex advantage to nonlinear electronic spectroscopy. Actually, we have already shown that the combination of femtosecond white light continuum and multichannel detection is very effective for two-photon absorption spectroscopy.[27,28] In the present Letter, we report a new multiplex SFG technique to measure interface-specific electronic spectra. We describe the details of the method and its application to a dye Nile Blue (NB) adsorbed at the air/water interface. The $\chi^{(2)}$ spectra of NB have a much better signal-to-noise ratio (*S*/*N*) and much denser spectral data points than the SHG spectra previously reported. It enables us to perform precise fitting analyses that can provide quantitative information about the electronic structure of NB at the interface.

Experimental Section. The setup and energy diagram of multiplex SFG for electronic $\chi^{(2)}$ spectroscopy are shown in Figure 1. A femtosecond Ti:sapphire regenerative amplifier (Spitfire, Spectra Physics) seeded by a femtosecond Ti:sapphire mode-locked oscillator (Tsunami, Spectra Physics) was used

10.1021/jp045306x CCC: $27.50
Published on Web 12/09/2004

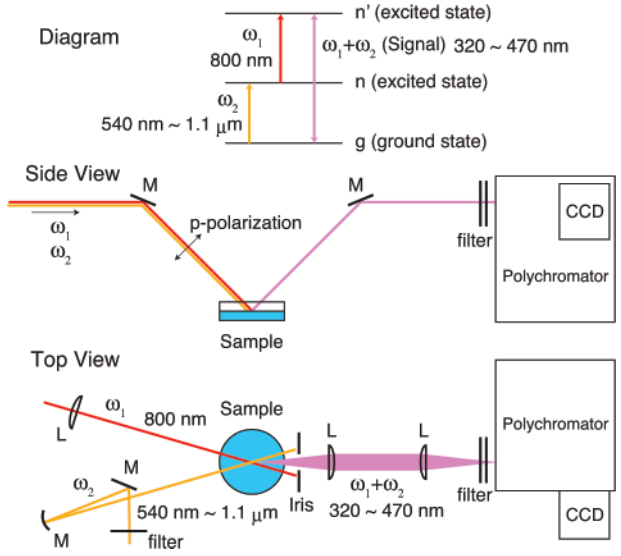

Figure 1. Energy diagram and experimental apparatus for electronic $\chi^{(2)}$ spectroscopy based on multiplex SFG. Labels L and M denote lens and mirrors, respectively. Some optical elements shown in the side (or top) view are not shown in the top (or side) view for clarity.

as a laser light source. A part of the regenerative amplifier output at 800 nm was focused into water flowing in a 5 mm cell, and the generated white light continuum was used as the ω_2 pulse. Wavelength components shorter than 540 nm in the white light continuum were eliminated by a color glass filter, because these components interrupted the detection of SFG signals: i.e., the spectrum of the ω_2 pulse extended from 540 nm to 1.1 μm. The other part of the amplifier output was attenuated and used as the ω_1 pulse. The center wavelength of the ω_1 pulse was 800 nm, and the bandwidth was 160 cm^{-1}. The ω_1 and ω_2 pulses were noncollinearly focused onto the same spot (ϕ 0.4 mm) at the air/water interface of a sample solution at an incident angle about 45° from normal. The angle between the ω_1 and ω_2 beams was set at about 10°. The linear polarization of the ω_1 and ω_2 beams was in the plane of reflection (i.e., p-polarization). The pulse energy for ω_1 was 14 μJ, and that for ω_2 was 6 μJ. Time delay between the ω_1 and ω_2 pulses was controlled by a translation stage. (We defined the time delay as positive when the ω_1 pulse reached the sample earlier.) The cross-correlation width of the ω_1 and ω_2 pulses was 200 fs. When the ω_1 and ω_2 pulses were temporally overlapped, sum frequency (SF) $\omega_1 + \omega_2$ was generated at the interface. An iris was put after the sample. The iris blocked the ω_1 and ω_2 pulses, but passed the whole $\omega_1 + \omega_2$ spectral components that diverged due to the phase matching condition. The SF light was collected and collimated by a plano-convex fused silica lens with UV antireflection (AR) coating, and it was focused by another identical lens onto the entrance slit of a single polychromator (HR-320, Jobin Yvon). The grating of the polychromator had 300 grooves per mm and 250 nm blaze wavelength. The spectrally dispersed SF light was detected by a thermoelectrically cooled CCD (Spec-10:256E, Roper Scientific) that had 1024 $\times$ 256 pixels. Unwanted scattering light was rejected by a dielectric filter and color glass filters in front of the polychromator. The typical exposure time of the CCD was 60 s.

A cylindrical quartz cell was used to contain the sample solution. NB was purchased from Aldrich (Nile Blue A perchlorate) and dissolved in distilled water without further purification. All the experiments were performed at room temperature, 299 K.

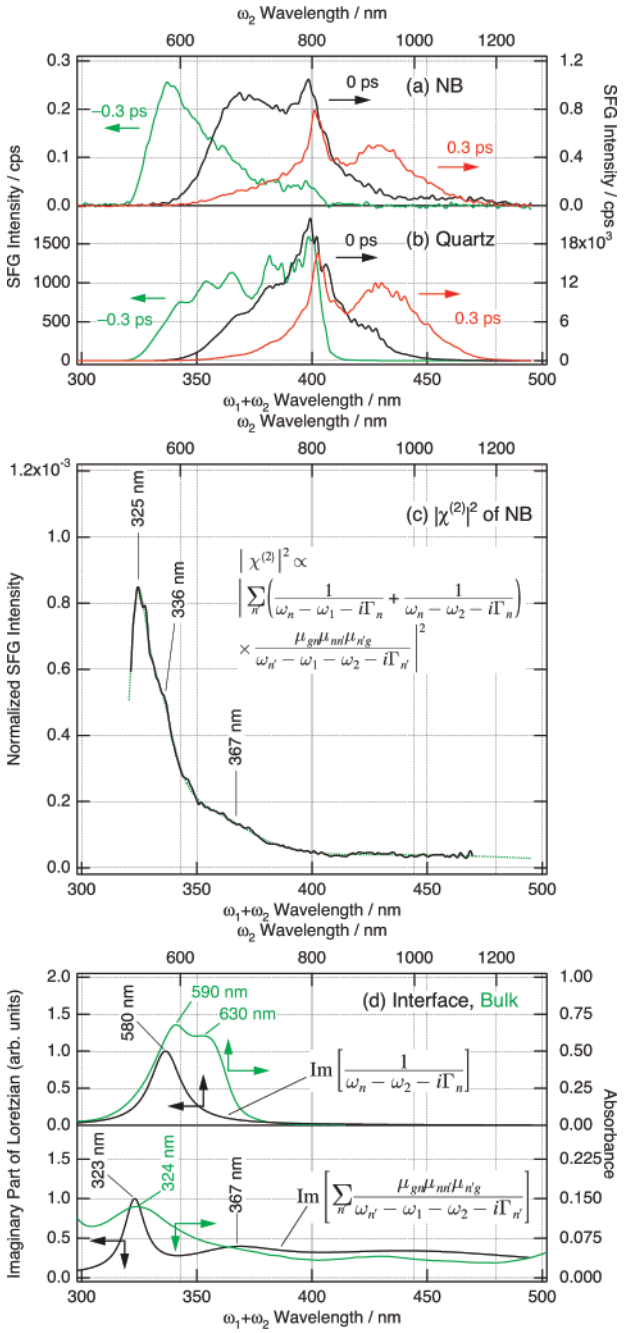

Figure 2. SFG spectra at time delay −0.3 (green curve), 0 (black curve), and 0.3 ps (red curve) of (a) NB at the air/water interface, and (b) the quartz wave plate. The left and right vertical axes stand for the CCD output count per second in parts a and b. The $|\chi^{(2)}|^2$ spectrum of NB (black line) and the fitting curve (green dotted line) are shown in part c. The imaginary parts of the one- and two-photon resonance Lorentz functions (calculated from the fitting results) are separately shown as black lines in part d together with the bulk UV−vis absorption spectrum of the same solution in a 2 mm cell (green line) for comparison. See text for the analysis details. The bottom and top horizontal axes represent wavelength corresponding to $\omega_1 + \omega_2$ and ω_2, respectively. The bulk concentration of the NB/water solution was 7.9×10^{-5} mol dm^{-3}.

Results and Discussion. Figure 2a shows the multiplex SFG spectra of NB at the air/water interface at time delay −0.3, 0, 0.3 ps. The bulk concentration of the NB/water solution was 7.9×10^{-5} mol dm^{-3}. Background signals originating from undesirable scattering light as well as CCD readout and dark charge noises have already been subtracted from these spectra. We used a spectrum at 20 ps as the background signals, because

it does not contain any SFG contribution. As shown in Figure 2a, the SFG spectrum depends on the time delay between the ω_1 and ω_2 pulses. It is due to optical chirp in the white light continuum (ω_2 pulse).[29] Time delay has to be positive in order to make the longer wavelength components of the ω_2 pulse overlapped temporally with the ω_1 pulse, because these components reach the sample spot earlier than the shorter wavelength components. We have found that measurements at the three time delay points (−0.3, 0, 0.3 ps) are necessary and sufficient to take advantage of the whole bandwidth of the ω_2 pulse. To obtain a physically meaningful $|\chi^{(2)}|^2$ spectrum for NB, we have to normalize the SFG spectra by standard data in the same way as done in multiplex IR−vis SFG[30] and coherent anti-Stokes Raman spectroscopy.[31] A quartz quarter-wave plate designed for 266 nm (Melles Griot) was chosen as the standard material, because it has a large $|\chi^{(2)}|$ value[32,33] and is transparent in the present wavelength region. (We can assume that $|\chi^{(2)}|$ of the quartz plate is independent of wavelength owing to its transparency.) The standard SFG spectra of the quartz plate was measured with the same experimental condition as that for NB, and are shown in Figure 2b. The normalization by the standard data corrects the distortion of the NB spectra due to the ω_2 spectral intensity, the effect of the ω_2 chirp, and the spectral sensitivity of the detection system. The normalized SFG spectra at −0.3, 0, and +0.3 ps were in good agreement with each other, and they were connected smoothly. The $|\chi^{(2)}|^2$ spectrum of NB at the air/water interface is shown as a black solid line in Figure 2c. As seen in this figure, the $|\chi^{(2)}|^2$ spectrum obtained has very high quality. It exhibits the intensity maximum at 325 nm. (The peak $|\chi^{(2)}|$ value for NB at 325 nm is estimated at 4.5×10^{-11} esu on the basis of the $|\chi^{(2)}|$ value of the quartz plate, 1.5×10^{-9} esu.[32,33]) In addition to this most prominent peak, two shoulder peaks are clearly recognized around 336 and 367 nm. These distinct spectral features indicate that at least three electronic transitions contribute to the spectrum. Such precise electronic spectra of interfacial molecules cannot be measured with the traditional scanning method.

We can acquire quantitative information on the electronic structure of NB at the interface by analyzing the $|\chi^{(2)}|^2$ spectrum. The high *S*/*N* and dense spectral data points of the $|\chi^{(2)}|^2$ spectrum enable us to perform a precise fitting analysis. The theoretical expression for $\chi^{(2)}$ in the present SFG experiment can be written as follows:[34]

$$\chi^{(2)} \propto \sum_{n,n'} \left(\frac{1}{\omega_n - \omega_1 - i\Gamma_n} + \frac{1}{\omega_n - \omega_2 - i\Gamma_n} \right) \frac{\mu_{gn}\mu_{nn'}\mu_{n'g}}{\omega_{n'} - \omega_1 - \omega_2 - i\Gamma_{n'}} \quad (1)$$

where μ_{ij} is the transition dipole matrix element between states i and j (where g stands for the ground state, n for a one-photon resonant excited state, and n′ for a two-photon resonant excited state), ω_i is the transition energy between the state g and i, and Γ_i is the line width of the transition. Note that the nondegeneracy of the incident photons is taken into account in eq 1, which is not necessary in the standard SHG $\chi^{(2)}$ expression[17] where ω_1 and ω_2 are set equal. We do not add a nonresonant background term to $\chi^{(2)}$ in eq 1, because NB gives resonant $\chi^{(2)}$ throughout the present wavelength region. Actually we did not observe any SFG signal without NB, which implies that the nonresonant background originating from the solvent is negligibly weak. We used the square modulus of eq 1 as the model function to perform the fitting analysis. All the matrix elements μ_{ij} were regarded as real in the analysis. (It is required by the time reversal symmetry.[35]) The converged fitting result is shown as a green dotted curve in Figure 2c. In the analysis, the following four transition energies (in wavelength) were necessary and sufficient to perfectly reproduce the data: for ω_n, 580 nm; for $\omega_{n'}$, 323, 367, and 448 nm.

Now we are able to discuss the electronic structure of NB at the air/water interface by making a comparison with that in bulk water. In Figure 2d, the bulk absorption spectrum of NB in water is compared with the $\chi^{(2)}$ Lorentz functions in eq 1 that are visualized in the following way: First, eq 1 is decomposed into one- and two-photon resonance parts. The former is

$$\frac{1}{\omega_n - \omega_2 - i\Gamma_n}$$

and the latter is

$$\sum_{n'} \frac{\mu_{gn}\mu_{nn'}\mu_{n'g}}{\omega_{n'} - \omega_1 - \omega_2 - i\Gamma_{n'}}.$$

The summation is not necessary for the one-photon part, because we obtained only one transition energy for ω_n. The imaginary parts of the one- and two-photon parts are plotted using the obtained fitting parameters along the wavelength axes corresponding to ω_2 and $\omega_1 + \omega_2$, respectively. We can regard these plots as the "interface absorption spectra". The peak at 323 nm for $\omega_1 + \omega_2$ in the interface absorption spectrum is nearly coincident with the bulk UV absorption peak at 324 nm. It straightforwardly indicates that the distinct 325 nm peak of the $|\chi^{(2)}|^2$ spectrum in Figure 2c is primarily attributed to the two-photon resonance at 323 nm. The shoulder of the $|\chi^{(2)}|^2$ spectrum at 336 nm is ascribed to the one-photon resonance at 580 nm (ω_1(800 nm) + ω_2(580 nm) = $\omega_1 + \omega_2$(336 nm)) that is 10 nm blue-shifted compared with the bulk absorption peak at 590 nm. The other transition energies, 367 and 448 nm for $\omega_{n'}$, make the broad resonance in the region of 350−500 nm for $\omega_1 + \omega_2$. The fitting analysis has clarified that both of the one- and two-photon resonances contribute to the spectral features of the $|\chi^{(2)}|^2$ spectrum. In fact, the slight red shift from the transition wavelength 323 nm to the observed $|\chi^{(2)}|^2$ peak wavelength 325 nm is brought about by the one-photon resonance contribution at 580 nm for ω_2.

Steinhurst and Owrutsky measured the SHG spectra of NB and other oxazine dyes at the air/water interface.[12] They investigated the solvent dependence and the effects of surfactants and salts, and concluded that the SHG signals originated almost exclusively from the dimers. In addition to the study of the interfacial dyes, they showed that the 590 and 630 nm peaks in the bulk absorption spectrum of NB (Figure 2d) were assigned to the dimer and the monomer, respectively. The present results support their conclusion. Actually, the fitting analysis for the $|\chi^{(2)}|^2$ spectrum indicates that only a single one-photon resonance exists at 580 nm. As shown in Figure 2d, this transition is safely correlated to the bulk dimer peak at 590 nm, but a transition corresponding to the bulk monomer peak at 630 nm is not recognized in the interface absorption spectrum. The precise spectrum obtained successfully confirm the primary contribution of the dimers from a purely spectroscopic viewpoint.

The concentration dependence of the $|\chi^{(2)}|^2$ spectrum was also investigated. Figure 3a shows the bulk UV−vis absorption spectra of NB/water in a 2 mm cell with two different concentrations. One is the same as for the sample in the above-described SFG measurement (7.9×10^{-5} mol dm^{-3}), and the

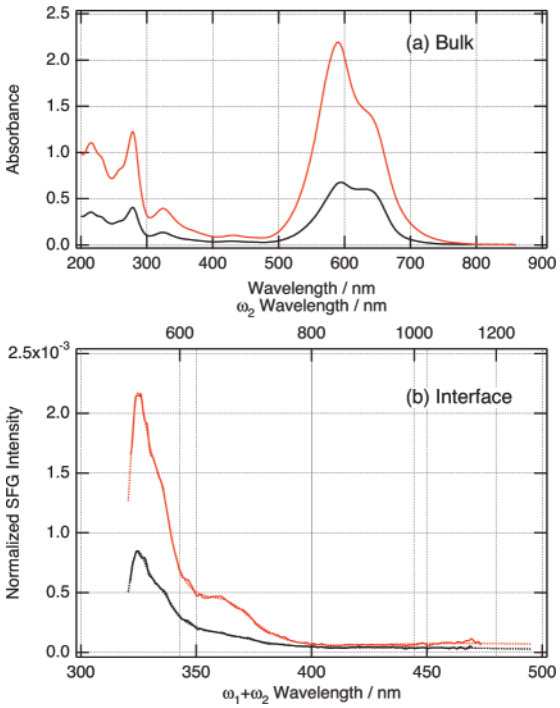

Figure 3. (a) UV−vis absorption spectra of NB in water for the saturated solution (red) and the 7.9×10^{-5} mol dm^{-3} solution (black). A 2 mm cell was used. (b) $|\chi^{(2)}|^2$ spectra of NB at the air/water interface (solid curves, data; dotted curves, fitting) for the saturated solution (red) and the 7.9×10^{-5} mol dm^{-3} solution (black).

other corresponds to the saturated solution ($\sim 2.4 \times 10^{-4}$ mol dm^{-3}). The absorption band shape in the region of 580−660 nm depends on the NB concentration, which is due to a monomer−dimer equilibrium in solution.[12] In fact, the dimer peak at 590 nm is more pronounced in the saturated-solution spectrum. We measured the electronic $|\chi^{(2)}|^2$ spectrum of the saturated solution, and the spectrum obtained is compared with that of the 7.9×10^{-5} mol dm^{-3} solution in Figure 3b. These $|\chi^{(2)}|^2$ spectra show that the spectral feature around the 325 nm peak is insensitive to the concentration, in contrast with the drastic change of the bulk band shape around 580−660 nm. It is consistent with the primary contribution of the dimers to the $\chi^{(2)}$ signals. It is noteworthy that a small peak is observed at 361 nm in the $|\chi^{(2)}|^2$ spectrum of the saturated solution. Because of this small peak, the saturated-solution spectrum is not reproduced by the fitting analysis that uses the same number of the parameters as for the 7.9×10^{-5} mol dm^{-3} solution. It indicates that a minor species appears at the air/water interface in the saturated solution. We found that the saturated-solution spectrum is reproduced well if we introduce one more transition energy as a fitting parameter in addition to the above-mentioned four energies. The converged fitting result, shown as a red dotted curve in Figure 3b, indicates additional one-photon resonance (ω_n) at 647 nm. Because the small peak becomes noticeable only under the high concentration condition, we tentatively attribute this minor species to an oligomer or an aggregate other than the dimer.

In conclusion, we obtained the electronic $|\chi^{(2)}|^2$ spectra of NB at the air/water interface by using the newly developed multiplex SFG technique. The high *S*/*N* and dense data points of the spectra obtained demonstrates a high potential of this technique as a standard method for electronic $\chi^{(2)}$ spectroscopy at interfaces.

Acknowledgment. Portions of this work were supported by a Grant-in-Aid for Young Scientists (B) (No. 15750023) from the Ministry of Education, Culture, Sports, Science, and Technology of Japan.

References and Notes

(1) Williams, C. T.; Beattie, D. A. *Surf. Sci.* **2002**, *500*, 545.
(2) Zhu, X. D.; Suhr, H.; Shen, Y. R. *Phys. Rev. B* **1987**, *35*, 3047.
(3) Ham, E. W. M. v. d.; Vrehen, Q. H. F.; Eliel, E. R. *Opt. Lett.* **1996**, *21*, 1448.
(4) Ritchter, L. J.; Petralli-Mallow, T. P.; Stephenson, J. C. *Opt. Lett.* **1998**, *23*, 1594.
(5) Hess, C.; Bonn, M.; Funk, S.; Wolf, M. *Chem. Phys. Lett.* **2000**, *325*, 139.
(6) Ishibashi, T.; Onishi, H. *Appl. Phys. Lett.* **2002**, *81*, 1338.
(7) Chang, Y. M.; Xu, L.; Tom, H. W. K. *Phys. Rev. Lett.* **1997**, *78*, 4649.
(8) Watanabe, K.; Takagi, N.; Matsumoto, Y. *Chem. Phys. Lett.* **2002**, *366*, 606.
(9) Fujiyoshi, S.; Ishibashi, T.; Onishi, H. *J. Phys. Chem. B* **2004**, *108*, 10636.
(10) Heinz, T. F.; Chen, C. K.; Ricard, D.; Shen, Y. R. *Phys. Rev. Lett.* **1982**, *48*, 478.
(11) Heinz, T. F.; Tom, H. W. K.; Shen, Y. R. *Phys. Rev. A* **1983**, *28*, 1883.
(12) Steinhurst, D. A.; Owrutsky, J. C. *J. Phys. Chem. B* **2001**, *105*, 3062.
(13) Castro, A.; Sitzmann, E. V.; Zhang, D.; Eisenthal, K. B. *J. Phys. Chem.* **1991**, *95*, 6752.
(14) Antoine, R.; Tamburello-Luca, A. A.; Hébert, P.; Brevet, P. F.; Girault, H. H. *Chem. Phys. Lett.* **1998**, *288*, 138.
(15) Zimdars, D.; Dadap, J. I.; Eisenthal, K. B.; Heinz, T. F. *Chem. Phys. Lett.* **1999**, *301*, 112.
(16) Benderskii, A. V.; Eisenthal, K. B. *J. Phys. Chem. A* **2002**, *106*, 7482.
(17) Steel, W. H.; Walker, R. A. *Nature (London)* **2003**, *424*, 296.
(18) Steel, W. H.; Lau, Y. Y.; Beildeck, C. L.; Walker, R. A. *J. Phys. Chem. B* **2004**, *108*, 13370.
(19) Shank, C. V.; Yen, R.; Hirlimann, C. *Phys. Rev. Lett.* **1983**, *51*, 900.
(20) Kemnitz, K.; Bhattacharyya, K.; Hicks, J. M.; Pinto, G. R.; Eisenthal, K. B.; Heinz, T. F. *Chem. Phys. Lett.* **1986**, *131*, 285.
(21) Sitzmann, E. V.; Eisenthal, K. B. *J. Phys. Chem.* **1988**, *92*, 4579.
(22) Sitzmann, E. V.; Eisenthal, K. B. *J. Chem. Phys.* **1989**, *90*, 2831.
(23) Meech, S. R.; Yoshihara, K. *Photochem. Photobiol.* **1991**, *53*, 627.
(24) Morgenthaler, M. J. E.; Meech, S. R. *Chem. Phys. Lett.* **1993**, *202*, 57.
(25) Shi, X.; Borguet, E.; Tarnovsky, A. N.; Eisenthal, K. B. *Chem. Phys.* **1996**, *205*, 167.
(26) Steinhurst, D. A.; Baronavski, A. P.; Owrutsky, J. C. *J. Phys. Chem. B* **2002**, *106*, 3160.
(27) Yamaguchi, S.; Tahara, T. *Chem. Phys. Lett.* **2003**, *376*, 237.
(28) Yamaguchi, S.; Tahara, T. *Chem. Phys. Lett.* **2004**, *390*, 136.
(29) Yamaguchi, S.; Hamaguchi, H. *Appl. Spectrosc.* **1995**, *49*, 1513.
(30) Ishibashi, T.; Onishi, H. *Appl. Spectrosc.* **2002**, *56*, 1298.
(31) Tahara, T.; Toleutaev, B. N.; Hamaguchi, H. *J. Chem. Phys.* **1994**, *100*, 786.
(32) Hagimoto, K.; Mito, A. *Appl. Opt.* **1995**, *34*, 8276.
(33) Shoji, I.; Kondo, T.; Kitamoto, A.; Shirane, M.; Ito, R. *J. Opt. Soc. Am. B* **1997**, *14*, 2268.
(34) Shen, Y. R. *The principles of nonlinear optics*; John Wiley & Sons: New York, 1984.
(35) Hamaguchi, H. The resonance effect and depolarization in vibrational Raman scattering. In *Advances in Infrared and Raman Spectroscopy*; Clark, R. J. H., Hester, R. E., Eds.; Wiley Heyden: London, 1985; Vol. 12; p 273.